ISSN 0018-1439, High Energy Chemistry, 2015, Vol. 49, No. 5, pp. 347–351. © Pleiades Publishing, Ltd., 2015.
Original Russian Text © A.E. Galashev, A.A. Galasheva, 2015, published in Khimiya Vysokikh Energii, 2015, Vol. 49, No. 5, pp. 389–393.

NANOSTRUCTURED SYSTEMS AND MATERIALS

Mercury Removal from Graphene by Bombardment with Xenon Clusters: Computer Simulation

A. E. Galashev and A. A. Galasheva

Institute of High Temperature Electrochemistry, Ural Division, Russian Academy of Sciences, ul. Sof'i Kovalevskoi 22, Yekaterinburg, 620137 Russia

e-mail: alexander-galashev@yandex.ru

Received January 16, 2015; in final form, March 3, 2015

Abstract—Molecular dynamics simulation of the bombardment of a target with a Xe_{13} cluster beam at energies of 5–30 eV and incidence angles of 0°–60° aiming to remove a mercury film from partially hydrogenated imperfect graphene has been performed. The graphene is completely cleaned of mercury at a cluster energy of $E_{Xe} \geq 15$ eV. It has been revealed that the mercury film tends to form a droplet. Mercury is removed from the graphene film via sputtering of single atoms and droplet detachment. The energy of interaction of mercury with graphene is very low and weakly depends on the incident beam energy. The horizontal mobility of atoms in the liquid metal film has a significantly higher value than their vertical mobility. A stress in graphene resulting from forces normal to the sheet plane is noticeably higher than that due to forces acting in its plane. Bombardment at an angle of incidence of 45° is more efficient than that at incidence angles of 0° and 60° and leads to lower graphene roughness.

DOI: 10.1134/S0018143915050057

Mercury thin film electrodes (MTFEs) are widely used for the anodic voltammetric determination of trace elements soluble in mercury [1]. The film is applied onto an inert substrate, typically a glassy carbon electrode. Mercury thin film electrodes can be prepared in a solution of pure mercury(II), after which the electrode is transferred to the test solution, or MTFEs can be fabricated in situ by simply adding mercury(II) ions to a medium to be analyzed. The mercury deposition rate is a function of the pH of the electrolyte, the deposition potential, the stirring speed, and the concentration of mercury ions. An optical study of MTFE has revealed the formation of both small and large droplets instead of having a uniform film [2].

Graphene, which is a two-dimensional (2D) honeycomb lattice of carbon atoms [3], is a promising material for electronics owing to rapid electron transport [4], a high specific surface area [5], and unusual properties [6]. Graphene was used to improve the limit of detection of metals [7, 8]. Graphene nanosheets were used in high-sensitivity sensors for the determination of lead and cadmium ions [9, 10]. The fact of charge transfer between graphene and metal ions, which makes the modified electrode much more sensitive, was established [11]. Graphene, transferred onto the surface of a glassy carbon electrode after mixing with a binder, can be successfully used to detect traces of heavy metals in water samples [10, 12]. Furthermore, the glassy carbon electrode prepared with the use of modified chemically reduced graphene oxide without a binder can be applied to determine Zn^{2+}, Cd^{2+}, and Pb^{2+} ions in water [13]. Repeated operation of the electrode requires its cleaning for removal of the deposited metals.

The wettability of graphene with mercury has not been studied yet. In this work, we examine a hypothetical mercury film on imperfect, partially hydrogenated graphene. However, the existence of such a film on graphene is quite realistic under certain conditions. Mercury typically does not wet the surface of most nonmetallic solids. At the same time, there is an evident transition from nonwetting to wetting by mercury on glass, quartz, or sapphire. Graphene sandwiched between a metal film and the substrate has a minimal effect on the interaction between them. Consequently, the mercury may spread over the graphene lying on glass, quartz, or sapphire. Multilayer graphene prepared by reduction of graphene oxide contains oxygenated functional groups on the basal planes and edges. Firm attachment of mercury at the functional-group sites can also lead to the formation of a mercury film on graphene. The electric field-induced wetting of graphene with mercury is also possible. By electrowetting, the carbon nanotube internal cavity is filled with mercury [14].

For targeted modification of the physical properties of the surface, argon and xenon ion beams are widely used. Xenon is heavier than argon almost by a factor of 3.3 and better suits for knocking out atoms of a heavy element, such as mercury. Faster Ar atoms (at the same beam energy) would lead to greater damage to the edges of graphene.

The objective of this study was to explore the possibility of graphene cleaning of mercury by bombardment with xenon clusters.

COMPUTER SIMULATION PROCEDURE

Interatomic interactions in graphene were expressed by a modified Tersoff many-body potential [15, 16]. The distance of covalent bonding was increased to 0.23 nm, and additional weak attraction at $r > 0.23$ nm defined by the Lennard-Jones (LJ) potential with the parameters as given in [17] was included. To eliminate the resulting torque at each lattice site of the graphene sheet, the rotational component of the force created by the atoms of adjacent sites was excluded. An analytical form of the local torsional interaction potential is given in [17].

Atomic interactions in the mercury film were simulated using the Schwerdtfeger pair potential [18]:

$$V_{\text{Sch}}(r) = U_{\text{Sch}}(\lambda r) = \sum_{j=3}^{9} a_2^* r^{-2j}, \quad (1)$$

where U_{Sch} is the original Schwerdtfeger potential for the mercury dimer [16], $\lambda = 1.167$ is used for adjusting to the density of liquid Hg at $T = 300$ K, and parameters a_{2j}^* are as given in [18].

The mercury–carbon and xenon–xenon interactions were defined by the LJ potential [18–20]. The interaction between Xe atoms and the target atoms (Hg and C) was defined by the pure repulsive ZBL potential [21]:

$$\Phi = Z_i Z_j \frac{e^2}{r}\left\{0.1818\exp\left(-3.2\frac{r}{a}\right) + 0.5099\exp\left(-0.9423\frac{r}{a}\right) + 0.2802 \times \exp\left(-0.4029\frac{r}{a}\right) + 0.02817\exp\left(-0.2016\frac{r}{a}\right)\right\}, \quad (2)$$

where Z_i and Z_j are the atomic numbers of the i th and j th atoms, e is the elementary charge, r is the distance between the atoms, and a is defined by the expression:

$$a = 0.8854 a_0 \left(Z_i^{0.23} + Z_j^{0.23}\right)^{-1}. \quad (3)$$

Here, a_0 is the Bohr radius. We neglect the weak attraction between Xe and Hg atoms on one hand and Xe and C atoms on the other hand, since the primary focus of this study is energy and momentum transfer, not chemical bonding [22].

Defects significantly enhance the adhesion of metals to graphene. Stone–Wales defects are common in graphene, each being represented by two contiguous five- and seven-membered rings. The graphene sheet used for the deposition of mercury had six defects of this kind with an approximately even distribution over its area. Hydrogenation was used to strengthen the graphene edges. The CH groups formed at the edges of the sheet were modeled by the single-atom scheme [23]. The C–CH and CH–CH interactions were expressed via the LD potential [23]. Partial functionalization of graphene in the form of attachment of hydrogen atoms to the edges stabilizes the structure, neither causing an increase in the interatomic distances nor creating roughness over the surface as a whole.

The mercury film on graphene was formed in a separate molecular dynamics (MD) calculation in two steps. In the first step, Hg atoms were placed over the centers of noncontiguous graphene cells so that the distance between Hg and C atoms would be equal to the distance 2.30 Å calculated by density functional theory [24]. On the loose mercury film consisting of 49 Hg atoms, other 51 Hg atoms were randomly deposited. Then, the system composed of 100 Hg atoms and 406 C atoms was equilibrated at 300 K in the MD calculation with a duration of 1 million time steps ($\Delta t = 0.2$ fs). The numerical solution of the equations of motion was performed by the fourth-order Runge–Kutta method. The target obtained in this way was then bombarded with icosahedral Xe_{13} clusters. Bombardment was performed in five series of 25 impacts each, as described in [25]. In computer simulation, the effectiveness of bombardment is reliably traced when the number of emitted ions is five to six times that of surface atoms to be moved [26]. In this numerical experiment, the number of projectile Xe atoms exceeds the number of Hg atoms by more than a factor of 16.

Bombardment at five different cluster energies of 5, 10, 15, 20, and 30 eV was performed using incident angles of $\theta = 0°$, 45°, and 60°. The complete graphene cleaning of mercury was reached at an angle of $\theta = 45°$ and a cluster beam energy of $E_{\text{Xe}} \geq 15$ eV. The bombardments at the other angles of incidence were significantly less effective and are not considered here. The heat released in the system (in both the metal film and graphene) by bombarding was partially dissipated by ejected Hg and Xe atoms and withdrawn using the Berendsen thermostat [27] included in the model.

The total self-diffusion coefficient of the atoms was calculated as

$$D = D_{xy} + D_z = \frac{1}{2\Gamma\tau}\left\langle\left[\Delta\mathbf{r}(t)\right]^2\right\rangle_n, \quad (4)$$

where $\Gamma = 3$ is the dimensionality of space. By $\langle\ldots\rangle$, averaging over n is denoted, where n is the number of time intervals τ for determination of $\left\langle\left[\Delta\mathbf{r}(t)\right]^2\right\rangle$.

The tensor components for stress existing in graphene were calculated through the kinetic energy of atoms at the elementary areas and the projection of forces acting on these areas [25].

The surface roughness (or arithmetic average roughness height) is defined by [28]

$$R_a = \frac{1}{N}\sum_{i=1}^{N}|z_i - \bar{z}|, \quad (5)$$

where N is the number of sites (atoms) on the graphene surface; z_i is the level of the ith atom; and $\overline{z}$ is the level of the graphene surface, with the values of z_i and $\overline{z}$ being determined in the same point of time.

The obtained value for the total energy of free single-sheet graphene at 300 K is −7.02 eV, which agrees with the results of quantum-mechanical calculation (−6.98 eV) [29]. The MD calculated value of the isochoric heat capacity of liquid mercury at this temperature is 28.4 J/(mol K) in agreement with the experimental value of 26.9 J/(mol K).

RESULTS AND DISCUSSION

To understand the behavior of the mercury film on graphene in the absence of bombardment, we calculated the system at 300 K using 10 million time steps. During this calculation, the Hg film transformed into a nearly spherical droplet with the flat base contacting the graphene. Convolving into the droplet was due to the strong attraction between the Hg atoms, as given by the Schwerdtfeger potential, compared with the attractive C–Hg interaction. During the bombardment of the target, mercury film also tended to form a droplet. After the bombardment with 5-eV Xe_{13} clusters, only a few Hg atoms significantly departed from the target and the dense "cloud" of mercury atoms and a small spherical droplet touching the substrate were formed over the graphene. The bombardment at an energy of 10 eV allowed a little more than half of the Hg atoms to be knocked off. An upward-stretched curved chain of Hg atoms appeared, as well as a small dense spheroid cluster with the "plume" of Hg atoms rising above it. The configuration shown in Fig. 1 corresponds to a cluster energy of 15 eV. It can be seen that during the bombardment, Hg atoms are removed from graphene mainly in two directions, sideways and upwards. Graphene has been almost completely cleaned of mercury, only single Hg atoms are held by the hydrogenated graphene edges. The further increase in the energy of Xe_{13} clusters leads to an even higher degree of removal, and both dense vapor and a droplet of mercury are formed over the graphene.

Figure 2 shows the interaction energies $E_{Hg–Hg}$ and $E_{C–Hg}$ obtained as a result of bombardment with different energies of Xe_{13} clusters. It can be seen that function $E_{Hg–Hg}(E_{Xe})$ is oscillatory, decreasing at $E_{Xe} = 30$ eV. The decrease is presumably due to the formation of a denser mercury droplet separated from graphene by the bombardment. At the same time, $E_{C–Hg}(E_{Xe})$ is a smooth function. The values of this function are close to zero; i.e., in general, very weak bonding between mercury and graphene is established using the impact of Xe_{13} clusters. A little stronger bond is manifested at an incident energy of xenon clusters of 15 eV when individual Hg atoms are retained by the hydrogenated graphene edges.

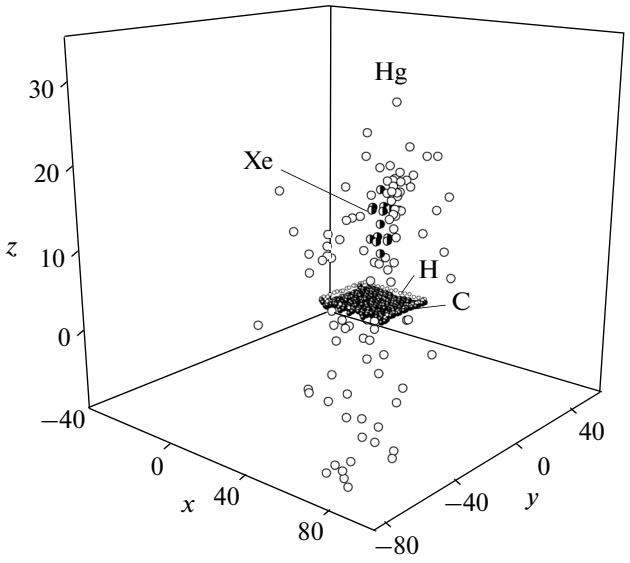

Fig. 1. Configuration of the "Hg film on graphene" target subjected to bombardment with 15-eV Xe_{13} clusters after 125 cluster impacts.

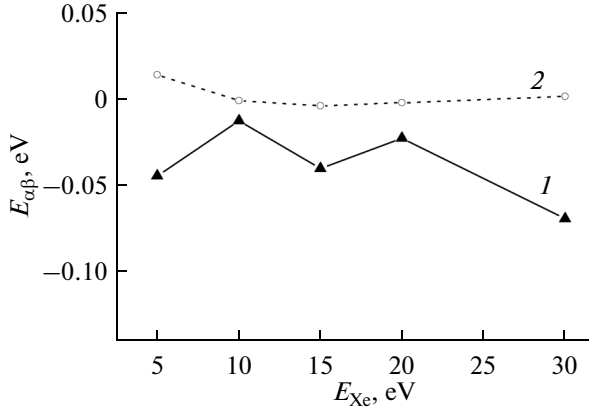

Fig. 2. Plots of (*1*) Hg–Hg and (*2*) C–Hg interaction energies obtained by performing five bombardment series with different energies of xenon clusters.

The horizontal D_{xy} and vertical D_z components of the diffusion coefficient of Hg atoms very weakly depend on the energy of the bombarding clusters (Fig. 3). This pattern of $D_{xy}(E_{Xe})$ and $D_{xy}(E_{Xe})$ plots is slightly different from that of similar functions characterizing the movement of Pb atoms during bombardment with Xe_{13} clusters at the same angle of incidence (45°). An essential difference for mercury is a higher value of component D_{xy} for all values of energy E_{Xe} (D_{xy} is more than fourfold greater than D_z). In the case of bombardment of the Pb film on graphene, the values of D_{xy} were moderately higher (up to 45%) than the corresponding D_z values. One of the causes of the discrepancy in the D_{xy} to D_z ratio between the mercury

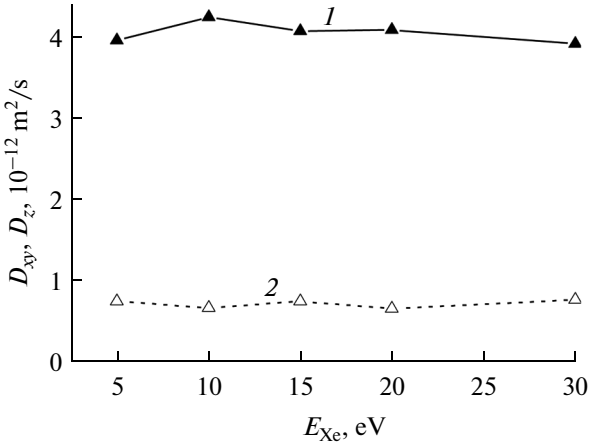

Fig. 3. Components (*1*) D_{xy} and (*2*) D_z of the self-diffusion coefficient of Hg atoms in the film, resulting from bombardment of the target with Xe_{13} cluster of different energies E_{Xe}.

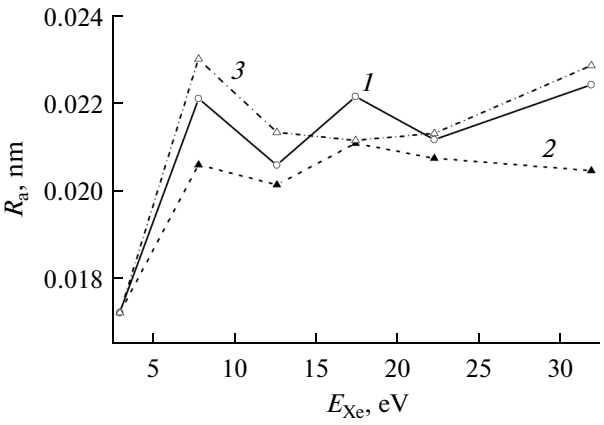

Fig. 5. Graphene roughness produced by target bombardment with Xe_{13} clusters at angles of incidence of (*1*) 0°, (*2*) 45°, and (*3*) 60°.

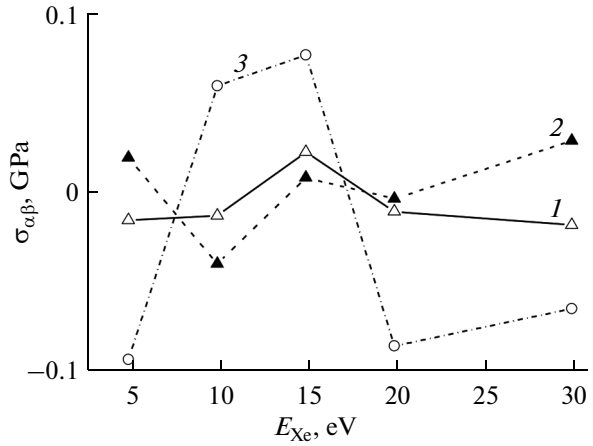

Fig. 4. Stress components (*1*) σ_{zx}, (*2*) σ_{zy}, and (*3*) σ_{zz} in the graphene plane, resulting from bombardment of the target with Xe_{13} clusters of different energies E_{Xe}.

and lead bombardments is a difference in the cooperative mechanisms of separation of heavy metals from graphene. There is the cluster or droplet mechanism of metal separation from the substrate surface along with the knocking out of single atoms in the case of mercury, whereas the "islet" mechanism of knocking out a collective of atoms is observed in the bombardment of the lead film. In other words, the flat "islet" of the Pb film is separated from the graphene and, being already in the free state, transforms into a spherical entity. The formation of the mercury droplet directly on the graphene surface is possible at higher values of the horizontal component of the mobility of metal atoms than in the case of lead film, which cannot convolve into a cluster. Another reason for the high values of D_{xy} for mercury relative to this mobility component for lead is that mercury occurs in the liquid state at temperatures reached during bombardment and lead is in the solid state.

Cluster bombardment affects the state of graphene. Figure 4 shows the dependence of stresses σ_{zx}, σ_{zy}, and σ_{zz} induced in the graphene plane upon the energy of clusters incident on the mercury–graphene target. The stresses (σ_{zx}, and σ_{zy} caused by the forces acting in the graphene plane are lower that the stresses produced by forces acting in the direction normal to the plane of the graphene sheet (σ_{zz}). The energy of 15 eV of Xe_{13} clusters, at which all of the three components of the stress tensor are positive, can be considered a threshold for the onset of complete graphene cleaning of mercury. The complex behavior of functions $\sigma_{\alpha\beta}(E_{Xe})$ is due to the presence on graphene of the Hg film, which can convolve into a droplet and vaporize as individual atoms, clusters, and droplets during bombardment.

Graphene roughness R_a is significantly (by 40–50%) increased by bombardment (Fig. 5). The value of R_a after the bombardment at a Xe_{13} cluster incident angle of 45° is always lower than that at an angle of $\theta =$ 0° or 60°. The graphene roughness acquires a maximal value at the "projectile" energy of $Xe_{13} = 15$ eV when the cluster bombardment is carried out at an angle of $\theta = 45°$ and $E_{Xe} = 30$ eV at the other angles of incidence. The bombardment at an angle of $\theta = 0°$ does not lead to acceptable graphene cleaning of mercury at any of the Xe_{13} cluster energies in the examined range (5–30 eV). In the case of cluster bombardment at an incidence angle of 60°, the complete removal of mercury from graphene was not achieved unless the cluster beam energy was 10 eV. Thus, graphene purification for the removal of mercury should be preferably performed by bombardment with Xe_{13} clusters at an angle of incidence of 45°, since the graphene acquires a minimum roughness in this case and mercury is

removed within a wider range of cluster beam energy (15–30 eV).

CONCLUSIONS

The bombardment of a mercury film on graphene with xenon clusters at an incidence angle of 0°–60° and an energy of 5–30 eV has been simulated. Graphene was freed from the mercury after 125 cluster impacts at $\theta = 45°$, starting with a beam energy of 15 eV. The tendency of the mercury film toward rolling into a droplet has been revealed. Mercury is removed from the graphene both as single atoms and in the form of a droplet, wherein the latter may be disintegrated during the bombardment. The mercury–graphene interaction energy is insignificant and very weakly depends on the energy of projectile xenon clusters. The horizontal component of the self-diffusion coefficient of mercury atoms is much greater than the vertical component, a difference that is due to the tendency of liquid mercury toward convolving into droplet. The stresses in the graphene plane induced by the forces normal to the plane are substantially higher than the stresses due to horizontal forces at any of the cluster beam energy examined. The roughness of graphene is markedly increased by cluster bombardment even at an incident beam energy as low as 5 eV; function $R_a(E_{Xe})$ exhibits an oscillatory behavior. Regardless of the incident beam energy considered, the mercury-coated graphene acquires the smallest roughness at an incidence angle of 45°. The hydrogenated graphene edges do not experience significant damage even after bombardment with a beam energy of 30 eV.

ACKNOWLEDGMENTS

This work was supported by the Russian Foundation for Basic Research, project no. 13-08-00273.

REFERENCES

1. Pinchin, M.J. and Newham, J., *Anal. Chim. Acta*, 1977, vol. 90, no. 1, p. 91.
2. Ertas, F.N., Gokcel, H.I., and Tural, H., *Turk. J. Chem.*, 2000, vol. 24, no. 3, p. 261.
3. Miao, F., Wijeratne, S., Coskun, U., Zhang, Y., and Lau, C.N., *Science*, 2007, vol. 317, no. 5844, p. 1530.
4. Xinran, W., Scott, M.T., and Hongjie, D., *J. Am. Chem. Soc.*, 2008, vol. 130, no. 26, p. 8152.
5. Yang, T., Li, F., Shan, C., Han, D., Zhang, Q., Niu, L., and Ivaska, A., *J. Mater. Chem.*, 2009, vol. 19, no. 26, p. 4632.
6. Galashev, A.E. and Rakhmanova, O.R., Physics-Uspekhi, 2014, vol. 57, no. 10, p. 970.
7. Fowler, J.D., Allen, M.J., Tung, V.C., Yang, Y., Kaner, R.B., and Weiller, B.H., *ACS Nano*, 2009, vol. 3, no. 2, p. 301.
8. Balandin, A.A., Ghosh, S., Bao, W., Calizo, I., Teweldebrhan, D., Miao, F., and Lau, C.N., *Nano Lett.*, 2008, vol. 8, no. 3, p. 902.
9. Li, J., Guo, S., Zhai, Y., and Wang, E., *Anal. Chim. Acta*, 2009, vol. 649, no. 2, p. 196.
10. Li, J., Guo, S., Zhai, Y., and Wang, E., *Electrochem. Commun.*, 2009, vol. 11, no. 5, p. 1085.
11. Khomyakov, P.A., Giovannetti, G., Rusu, P.C., Brocks, G., van den Brink, J., and Kelly, P.J., *Phys. Rev. B*, 2009, vol. 79, no. 19, p. 195425.
12. Willemse, C.M., Tlhomelang, K., Jahed, N., Baker, P.G., and Iwuoha, E.I., *Sensors*, 2011, vol. 11, no. 4, p. 3970.
13. Zbeda, S., Pokpas, K., Titinchi, S., Jahed, N., Baker, P.G., and Iwuoha, E.I., *Int. J. Electrochem. Sci.*, 2013, vol. 8, no. 9, p. 11125.
14. Chen, J.Y., Kutana, A., Collier, C.P., and Giapis, K.P., *Science*, 2005, vol. 310, no. 5753, p. 1480.
15. Tersoff, J., *Phys. Rev. Lett.*, 1988, vol. 61, no. 25, p. 2879.
16. Galashev, A.E., Polukhin, V.A., Izmodenov, I.A., and Rakhmanova, O.R., *Glass Phys. Chem.*, 2007, vol. 33, no. 1, p. 86.
17. Stuart, S.J., Tutein, A.V., and Harrison, J.A., *J. Chem. Phys.*, 2000, vol. 112, no. 14, p. 6472.
18. Kutana, A. and Giapis, K.P., *Nano Lett.*, 2006, vol. 6, no. 4, p. 656.
19. Kim, Y.M. and Kim, S.-C., *J. Korean Phys. Soc.*, 2002, vol. 40, no. 2, p. 293.
20. Li, F.-Y. and Berry, R.S., *J. Phys. Chem.*, 1995, vol. 99, no. 9, p. 2459.
21. Ziegler, J.F., Biersack, J.P., and Littmark, U., *Stopping and Ranges of Ions in Matter*, New York: Pergamon, 1985, vol. 1.
22. Delcorte, A. and Garrison, B.J., *J. Phys. Chem. B*, 2000, vol. 104, no. 29, p. 6785.
23. Lamari, F.D. and Levesque, D., *Carbone*, 2011, vol. 49, no. 15, p. 5196.
24. Wilcox, J., Sasmaz, E., and Kirchofer, A., *J. Air Waste Manag. Assoc.*, 2011, vol. 61, no. 4, p. 418.
25. Galashev, A.E. and Galasheva, A.A., *High Energy Chem.*, 2014, vol. 48, no. 2, p. 112.
26. Inui, N., Mochiji, K., and Moritani, K., *Nanotechnology*, 2008, vol. 19, no. 50, p. 505501.
27. Berendsen, H.J.C., Postma, J.P.M., van Gunsteren, W.F., et al., *J. Chem. Phys.*, 1984, vol. 81, no. 8, p. 3684.
28. Galashev, A.E. and Galasheva, A.A., *High Energy Chem.*, 2015, vol. 49, no. 2, p. 122.
29. Davydov, S.Yu., *Phys. Solid State*, 2012, vol. 54, no. 4, p. 875.

Translated by S. Zatonsky